CONF-9707110--2

Silicon and Zinc Telluride Nanoparticles Synthesized by Pulsed Laser Ablation: Size Distributions and Nanoscale Structure

Douglas H. Lowndes,* Christopher M. Rouleau,* T. Thundat,‡
G. Duscher*, E. A. Kenik,# and S. J. Pennycook*

Oak Ridge National Laboratory, P. O. Box 2008, Oak Ridge, TN 37831-6056

* Solid State Div. ‡ Life Sciences Div. # Metals and Ceramics Div.

Submitted to:
The Fourth International Conference on Laser Ablation (COLA '97)
Asilomar Conference Center,
Monterey Bay, California
July 21–25, 1997

August 1997

Prepared by
Solid State Division
Oak Ridge National Laboratory
P.O. Box 2008
Oak Ridge, Tennessee 37831-6056
managed by
LOCKHEED MARTIN ENERGY RESEARCH CORP.
for the
U.S. DEPARTMENT OF ENERGY
under contract DE-AC05-96OR22464

DISCLAIMER

Silicon and Zinc Telluride Nanoparticles Synthesized by Pulsed Laser Ablation: Size Distributions and Nanoscale Structure

Douglas H. Lowndes,* Christopher M. Rouleau,* T. Thundat,‡
G. Duscher*, E. A. Kenik,# and S. J. Pennycook*

Oak Ridge National Laboratory, P. O. Box 2008, Oak Ridge, TN 37831-6056

* Solid State Div. ‡ Life Sciences Div. # Metals and Ceramics Div.

Corresponding author:
Douglas H. Lowndes, Solid State Division, Bldg. 3150,
Oak Ridge National Laboratory, P. O. Box 2008, Oak Ridge, TN 37831-6056
Tel.: (423) 574 - 6306 Fax: (423) 576 - 3676 e-mail: vdh@ornl.gov

PACS Classifications

61.46.+w	Solid clusters and nanoparticles
78.55.Et	II-VI semiconductors (photoluminescence)
81.15.Fg	Laser ablation technique
81.35.+k	Granular materials: aggregation characteristics

Key Words

pulsed laser ablation	size distribution
pulsed laser deposition	atomic force microscopy
Si	scanning electron microscopy
ZnTe	transmission electron microscopy
nanoparticle	Z-contrast
nanocrystal	

This research was sponsored by the Oak Ridge National Laboratory, managed by Lockheed Martin Energy Research Corp., for the U.S. Department of Energy, under contract DE-AC05-6OR22464.

Silicon and Zinc Telluride Nanoparticles Synthesized by Pulsed Laser Ablation: Size Distributions and Nanoscale Structure

Douglas H. Lowndes,* Christopher M. Rouleau,* T. Thundat,‡
G. Duscher*, E. A. Kenik,# and S. J. Pennycook*

Oak Ridge National Laboratory, P. O. Box 2008, Oak Ridge, TN 37831-6056
* Solid State Div. ‡ Life Sciences Div. # Metals and Ceramics Div.

Abstract

Size distributions of Si and ZnTe nanoparticles produced by low energy density ArF (193 nm) pulsed laser ablation into ambient gases were measured as a function of the gas pressure and target-substrate separation, D_{ts}, using atomic force microscopy (AFM) and high resolution scanning electron microscopy (HRSEM). For low energy density (Ed = 1.04 J/cm^2) ablation of Si into He at pressures of 0.5, 1.5, 4 and 10 torr, large nanoparticles were most numerous at D_{ts} = 10 mm, with smaller nanoparticles found at 20 mm and 40 mm. For each D_{ts} value a maximum of the mean nanoparticle diameter occurred for a He pressure near 6 torr, in contrast to other recent measurements in which the size of Si nanoparticles increased monotonically with the He pressure. High resolution Z-contrast transmission electron microscopy (HRZTEM) and electron energy loss spectroscopy (EELS) revealed that ZnTe nanoparticles formed by ablation into nitrogen at E_d = 0.74 J/cm^2 consisted of a crystalline ZnTe core surrounded by an amorphous ZnO shell. Growth defects and surface steps were clearly visible in the ZnTe crystalline core. The dependences of the mean diameter of ZnTe nanocrystals on nitrogen pressure and D_{ts} were qualitatively similar to those found for Si in He.

1. Introduction

Recent pulsed laser deposition (PLD) experiments have demonstrated that by varying the pulsed laser wavelength, intensity, and ambient gas pressure, both the energy distribution and the nature of the ablated flux can be controlled [1, 3–12]. Cluster and nanocrystal formation are greatly enhanced by ablating a material into a moderate-pressure (0.1–10 torr) ambient gas [2]. With increasing gas pressure, the film-deposition flux changes from primarily atoms and ions to clusters and nanocrystals, the latter typically having diameters of 1 to 20 nm and containing from 10^2 to 10^6 atoms. For example, we recently grew p-type, nitrogen-doped epitaxial ZnTe films on GaAs(001) by ablating a ZnTe target into ambient N_2 gas [3–5]. However, the hole mobility exhibited a pronounced maximum in films grown at ~ 50 mtorr N_2 pressure, with lower mobilities for films grown at N_2 pressures ≥100 mtorr. This degradation was shown to be due to the onset of significant ZnTe cluster deposition with increasing N_2 pressure [4, 5].

Pure cluster-assembled or nanocrystalline films are of interest in their own right since they may have properties much different than films grown from a predominantly atomic/ionic flux, either because of quantum confinement effects or because entirely new composite materials can be formed, for example by reaction with species present in the vapor phase [6]. Thin-film deposits of nanocrystalline Si were grown recently by Yoshida et al. [7–9], by ablating a Si-wafer target into He gas at a low pulsed ArF (193 nm) laser energy density, E_d, of 1 J/cm^2, and also by Makimura et al. [10–12], who used a frequency-doubled Nd:YAG (532 nm) laser at much higher E_d ~ 10 J/cm^2. Much smaller nanocrystals were obtained for ablation into He than into Ar [13, 14]. Using a target-substrate separation, D_{ts}, of 7 mm, Yoshida et al. found that the mean size of the Si nanocrystals increased proportional to the 1/2.8 power of the He pressure, P, for $2 \leq P \leq 10$ torr [7]. Using D_{ts} = 19 mm,

Makimura et al. found qualitatively similar behavior, with the Si nanocrystal diameter varying as the 1/1.3 power of P for $0.5 \leq P \leq 20$ torr [10].

Because of interest in using PLD for both epitaxial and nanocrystalline semiconductor film growth, and the importance of understanding cluster and nanoparticle formation, we have carried out systematic studies of the conditions required to form (or to avoid forming) highly nanocrystalline semiconductor films. Here we report measurements of the size distributions and microstructure for Si and ZnTe nanocrystals produced by pulsed ArF (193 nm) laser ablation into ambient He or N_2, respectively. The mean nanocrystal size was controlled by varying both the ambient gas pressure and the target-substrate separation. For nano-Si, our experimental conditions were chosen to overlap, but extend to larger D_{ts}, the recent low-E_d experiments by Yoshida et al. that produced electroluminescent nano-Si films [9]. For nano-ZnTe, the experimental conditions overlap but extend to much higher nitrogen pressures and shorter D_{ts} the low-E_d ablation condition that we earlier found was best for epitaxial growth of p-ZnTe:N [3-5].

2. Experimental

Nanoparticles were deposited at room temperature onto Si(001) substrates (Wacker, both p- and n-type, 0.2-0.3 ohm-cm) in a load-locked UHV chamber. For each deposition, two Si strips (4 mm wide x 40 mm long) were positioned D_{ts} from the target. The two Si strips were mounted one above the other, facing the target, with a 5 mm gap between them through which the laser beam could pass. The Si substrates were dipped for 30 sec in 5% HF (to reduce the native oxide and hydrogen-passivate the surface), blown dry with N_2, and then were immediately loaded into the chamber.

A short-wavelength ArF (193 nm) laser was used at low energy density, E_d, in order to minimize ejection ("splashing") of large particulates from the targets. A 10 mm x 10 mm aperture was used to select the most uniform part of the laser beam,

which was focused using two crossed cylindrical lenses. E_d was carefully calibrated using burn patterns on tempered, polished, and blued steel ribbon [16]; the focused beam area was ~5.4 mm^2. Targets were rotated at 20 rpm and the laser beam also was switched from the left to the right side of the target after every 128 shots (making a ~12 mm diam track) to minimize target "coning" and production of large particulates. In connection with model calculations it should be noted that all targets were pre-ablated to reach a steady state (and a textured surface) prior to nanoparticle deposition by taking 2,000 or more shots in vacuum while the substrates were in the load lock.

Silicon. Nanoparticles were deposited using 500 laser shots on Si(001) targets (Wacker, p-type, 0.2-0.3 ohm-cm) at a pulse energy of 56 mJ, corresponding to E_d = 1.04 (±0.06) J/cm^2, in order to closely reproduce the laser conditions of Yoshida et al. [7-9]. An ablation threshold E_d^{th} ~ 0.76 J/cm^2 was determined by observing the onset of visible Si plume formation in 1 torr He. This E_d^{th} value may be useful to scale model calculations of nanoparticle formation to the deposition conditions used here. Nanoparticles were collected for static (no flow) He (99.9999% pure) pressures P = 0.5, 1.5, 4 and 10 torr at target-substrate distances D_{ts} = 10, 20, and 40 mm.

ZnTe. Nanoparticles were deposited using 500 laser shots on a fine-grained, hot-pressed ZnTe target (starting material 99.999% pure) at a pulse energy of 40 mJ, corresponding to E_d = 0.74 J/cm^2. This is close to the laser E_d used for our best p-ZnTe:N epitaxial films, grown in 50 mtorr of N_2 [3-5]. ZnTe nanoparticles were collected at distances 4 cm ≤ D_{ts} < 12 cm from the target, at N_2 pressures of 0.15, 1.5 and 10 torr; hydrogen was used in a few experiments.

Size Distribution Measurements. Images of the nanoparticles were obtained using a high-resolution (field emission) scanning electron microscope (HRSEM, Philips XL30/FEG) in secondary electron mode. The nominal probe size for the 20-

kV condition used is ~2-3 nm, allowing detection (though not measurement) of nanoparticles with diameters approaching that limit. For conditions that produced large (10-20 nm) ZnTe nanoparticles, their size distributions were determined by direct measurements of ~140 nanoparticles in the HRSEM images. The heights (~diameters) of nanoparticles too small for accurate HRSEM measurements (all Si and some ZnTe) were determined from tapping-mode atomic force microscope (TM-AFM, Nanoscope III, Digital Instruments, Santa Barbara, CA) images of 500 nm-square areas in two different regions of each specimen; these regions are believed to correspond to the center and left-of-center parts of the ablation plume. The TM-AFM has good vertical resolution ~ 0.05 nm but its horizontal resolution (apparent particle width) is limited by the finite size of the imaging tip. Consequently, the measured nanoparticle height was taken to be the nanoparticle diameter. Nanoparticle size distributions (number density vs diameter) were obtained by statistical analysis of the TM-AFM images. Briefly, the images first were fit to a plane and flattened; then a statistical roughness analysis was carried out to determine the rms and average surface roughnesses. A grain size analysis was performed next by passing a series of planes through the nanoparticles at various heights above the reference surface, using a height increment of one-half the rms surface roughness. The number of nanoparticles terminating in each height interval then could be determined. This method of determining the nanoparticle size distribution tends to overestimate the number of very small nanoparticles because jagged surfaces on larger particles may be counted as two (or more) particles. In contrast, direct visual analysis of plan-view HRSEM images inevitably *under*estimates the number of small particles, because particles below a certain size are ignored. Jaggedness also could result in an overestimate of the number of large particles, but that error can be avoided simply by viewing successive planar intersections and noting where bifurcations occur. The nanoparticle height

distribution also was viewed along particular line-scan directions on the surface as a rough check on each statistical analysis.

3. Results for Silicon

Representative AFM measurements of the Si nanoparticle size distribution (nanoparticles/μm^2 vs mean height) are shown in Figure 1. Similar measurements [16] revealed that for He pressures in the range $1.5 \leq P \leq 10$ torr, large nanoparticles were most numerous close to the target. With increasing target-substrate separation, the size distribution shifts toward smaller nanoparticles.

If each distribution is characterized by the average nanoparticle diameter then the results shown in Figures 2 are obtained. For all target-substrate separations in the range $10 \leq D_{ts} \leq 40$ mm, the mean Si nanoparticle size was maximized for $P \sim 6$ torr under these ablation and deposition conditions. The existence of a maximum in the size distribution as a function of pressure is in striking contrast to the results of Yoshida et al. [7] and of Makimura et al. [10], who found that the mean diameter of Si nanoparticles increased monotonically with the He pressure in this pressure range, as is also shown in Fig. 2.

When combined with visual observations of the ablation plume the AFM data reveal that for any He pressure the largest nanocrystals were deposited beyond, but still close to, the end of the luminescent plume, with the nanocrystal size distribution shifting systematically toward smaller average diameters for larger D_{ts} (Figs. 1 and 2). This trend does not seem to have been present (or noticed) in earlier studies of laser-ablated Si nanocrystals. However, it is quite general in our data and perhaps is a useful constraint on model calculations of the overall nanocrystal formation and deposition process.

4. Results for Zinc Telluride

Table 1 shows that by changing the N_2 or H_2 pressure and target-substrate separation the average diameter of ZnTe nanoparticles could be varied over a wide

range. Quite small ZnTe nanocrystals, with mean diameters of 1–2 nm, were formed either by ablating into N_2 at 150 mtorr or into H_2 at 1 torr and collecting at D_{ts} = 10 cm (Table 1).

HRSEM data for P[N_2] = 1.5 torr (Table 1) show that for fixed pressure the largest ZnTe nanocrystals were collected closest to the ablation target, just as was found for Si (Figs. 1 and 2). The HRSEM data for N_2 pressures of 1.5 and 10 torr and fixed D_{ts} = 4 cm also reveal slightly smaller ZnTe nanocrystals at the higher pressure, perhaps indicating that the mean size of ZnTe nanocrystals reaches a maximum value at an intermediate N_2 pressure, similar to the behavior of Si shown in Fig. 2.

Table 1 also includes a comparison of the ZnTe nanocrystal diameters measured by HRSEM and AFM for P[N_2] = 1.5 torr, D_{ts} = 8 cm, and shows that the mean diameter determined by AFM is about a factor of two smaller. This does not indicate that there would be any difference in the diameters measured by AFM and HRSEM for the same nanocrystal, but simply that the AFM data set includes many small nanocrystals that apparently are missed in visual inspections of HRSEM images.

HRZTEM was used to study in detail the microstructure, crystallinity, and composition of individual ZnTe nanoparticles in relation to their formation mechanism. The samples for these studies were briefly air-exposed but were loaded into the microscope within a few minutes after deposition. As shown in Figure 3, atomic-resolution Z-contrast imaging revealed that both large (~10 nm) and small ZnTe (~2–3 nm) nanoparticles consist of a crystalline core surrounded by an amorphous ZnO shell (see EELS below) [17]. In fact, Z-contrast imaging detected what appear to be facets at the surface of the crystalline core as well as internal defect structures, including what may be a twin boundary and stacking faults within the larger nanocrystal in Fig. 3. Other AFM images, as well as HRSEM pictures, revealed

that the largest ZnTe nanocrystals were formed by collisions in the N_2 gas that resulted in initial nano-crystallite growth followed by subsequent agglomeration with other nanocrystals.

Information about the electronic structure and chemical composition of ZnTe nanocrystals was obtained by measuring electron energy loss spectra (EELS) point-by-point across the larger nanocrystal of Fig. 3(top). The resulting high–resolution composition profile is shown in Fig. 3(bottom). The O and Te EELS profiles and HRZTEM images reveal definitively that the nanocrystal has a crystalline ZnTe core surrounded by an oxidized, amorphous ZnO outer shell.

5. Discussion

Our finding that there is a maximum in the Si nanoparticle size distribution for P[He] ~ 6 torr is contrary to two earlier results [7, 10]. This difference may be due to the relatively low laser E_d(193 nm) = 1.04 (±0.06) J/cm^2 or the different collection geometry that was used in this work. Makimura et al. used a much higher E_d(532 nm) ~ 10 J/cm^2 to produce Si nanoparticles with mean diameters very similar to those reported here, as shown in Fig. 2. In contrast, Yoshida et al. used nominally the same E_d(193 nm) ~ 1 J/cm^2 to produce much larger Si nanoparticles at a D_{ts} of only 7 mm, their mean diameters increasing from >10 nm for P[He] = 2.5 torr to ~20 nm at 10 torr (see Fig. 2).

The relatively "open" collection geometry employed in this work, with long Si-strip substrates placed both above and below a central ~5 mm gap through which the laser beam passed, may reduce reflection of the shock front that is formed when a target is ablated into a gas [18]. In the experiments of Yoshida et al., at nominally the same E_d as here, the reflection of this shock front back into itself by the uninterrupted substrate surface may have enhanced formation of clusters and larger nanocrystals. However, another possible cause for the different pressure dependences is that a significantly higher E_d than 1 J/cm^2 may have been used in

the experiments by Yoshida et al.. Their E_d was estimated from the pulse energy measured in front of the entry window and the laser burn area on Polaroid film [13]; the latter is susceptible to overestimating the laser spot size and therefore underestimating E_d. There is clear evidence of a difference between the two sets of experiments since Yoshida et al. deposited a ~150-nm thick nano-Si film in about 30 minutes at 10 Hz [13], while our deposition rate was much lower using E_d = 1.04 J/cm^2. Indeed, for the film–deposition experiments of Yoshida et al. the laser E_d may have been ~1.8 J/cm^2, or even higher [13].

The absence of a normal (Gaussian) size distribution in the AFM measurements of Fig. 1, in contrast to HRSEM measurements, seems to result from the ability of the AFM to detect quite small nanoparticles, together with the need for an absolute cutoff (at approximately one standard deviation in surface roughness) in the minimum nanoparticle size that can be measured by the statistical analysis method used here.

The largest Si nanoparticles were found at D_{ts} = 10 mm in this work, with the mean diameters decreasing at D_{ts} = 20 mm and 40 mm (Fig. 2). Yoshida et al. did not vary D_{ts} [13], while the model of Makimura et al. [10] suggests that the nanoparticle size should increase with increasing D_{ts} if D_{ts} lies inside the "final" (stationary) position of plume luminescence, but should be approximately constant if D_{ts} lies outside. Matsunawa et al. reported an increase in the mean size of metallic nanoparticles formed by millisecond pulsed Nd:YAG laser ablation in 1 atm. of Ar out to D_{ts} ~ 15 mm, with the metallic nanoparticles linking together but maintaining a similar size distribution at larger distances [14]. The fact that we found very few nanoparticles at any location in the 10-40 mm range for P[He] = 0.5 torr, but easily measurable distributions for P[He] ≥ 1.5 torr, suggests that the primary region of nanoparticle formation and aggregation (corresponding to the "final" luminescence position in the model of Makimura et al. [10]) lay beyond our

substrates at P[He] = 0.5 torr. This is in qualitative agreement with our visual observations of a bright, orange fluorescent ablation plume extending more than 20 mm out from the Si target at P[He] = 0.5 torr [16]. Thus, the collection of few Si nanoparticles in our experiments at P[He] = 0.5 torr agrees qualitatively with the model of Makimura et al.. The decreasing Si nanoparticle size we observed for D_{ts} of 20 mm and 40 mm (Figs. 1 and 2) may simply reflect a rapidly decreasing ablation flux and nucleation rate with increasing D_{ts} for the low-E_d condition used here.

With regard to the crystallinity of Si nanoparticles, Yoshida et al. found that cross-sectional HRTEM images of ~ 3-nm and ~ 10-nm diameter spherical Si particles revealed a core containing lattice planes with a spacing of 0.31 nm, nearly equal to the spacing of the (111) planes in crystalline Si. The core was surrounded by amorphous carbon from the microscope grid on which the nanoparticles were deposited [7]. Thus, at least the cores of the generally larger Si nanoparticles produced by Yoshida et al. were crystalline. As described above, we found a similar structure for ZnTe nanocrystals of various sizes. Whether the smaller Si nanoparticles produced in our work have a crystalline Si core surrounded by an oxide shell, as argued by Makimura et al., is uncertain [10]. We note that Duscher and co-workers [19] recently found that the most luminescent laser-ablated Si nanoparticles were a homogeneous silicon-rich oxide, and definitely did not have a crystalline core with an oxide shell structure such as that reported here for ZnTe (Fig. 3).

6. Conclusions

Several significant conclusions follow from this work. First, the mean size of nanoparticles produced by ablation into a gas and collected at some fixed distance does not necessarily increase monotonically with the gas pressure, as was found in earlier work [7, 10]. Instead, for silicon ablated into helium the mean nanoparticle size reached a maximum at a pressure near 6 torr, with smaller nanoparticles found

at both higher and lower pressures, for each target-substrate separation studied. Data for ZnTe ablated into nitrogen show qualitatively the same behavior. Second, within the region in which nanoparticles can be found (beginning near the end of the luminescent plume and beyond), the largest nanoparticles are found close to the target with the mean nanoparticle size decreasing at greater distances. (However, few to no nanoparticles were found very close to the target, i.e. within the luminescent plume.) Third, HRZTEM measurements reveal that both large and small ZnTe (and presumably other compound semiconductor) nanoparticles have a crystalline ZnTe core. Fourth, systematic differences in average nanoparticle diameters determined by AFM and HRSEM apparently result simply from AFM's ability to detect smaller particles, i.e. the AFM data set extends to smaller values. Finally, the mean size of nanoparticles produced by ablation into a gas is a strong function of the gas molecules' atomic number (scattering cross section), with larger molecules producing larger nanoparticles at a given pressure.

Acknowledgments

The authors thank P. H. Fleming for assistance with analysis of the HRSEM nanoparticle images. This research was sponsored by the Oak Ridge National Laboratory, managed by Lockheed Martin Energy Research Corp. for the U.S. Department of Energy under contract DE-AC05-96OR22464.

References

[1] D. H. Lowndes, D. B. Geohegan, A. A. Puretzky, D. P. Norton, and C. M. Rouleau, *Science* **273**, 898 (1996).

[2] D. E. Powers et al., *J. Phys. Chem.* **86**, 2556 (1982).

[3] C. M. Rouleau, D. H. Lowndes, J. W. McCamy, J. D. Budai, D. B. Poker, D. B. Geohegan, A. A. Puretzky, and S. Zhu, *Appl. Phys. Lett.* **67**, 2545 (1995).

[4] D. H. Lowndes, C. M. Rouleau, D. B. Geohegan, A. A. Puretzky, M. A. Strauss, A. J. Pedraza, J. W. Park, J. D. Budai, and D. B. Poker, *Mater. Res. Soc. Symp. Proc.* **397**, 107 (1996).

[5] C. M. Rouleau, D. H. Lowndes, M. A. Strauss, S. Cao, A. J. Pedraza, D. B. Geohegan, A. A. Puretzky, and L. F. Allard, *Mater. Res. Soc. Symp. Proc.* **397**, 119 (1996).

[6] W. M. K. P. Wijekoon, M. Y. M. Lyktey, P. N. Prasad, and J. F. Garvey, *Appl. Phys. Lett.* **67**, 1698 (1995).

[7] T. Yoshida, S. Takeyama, Y. Yamada, and K. Mutoh, *Appl. Phys. Lett.* **68**, 1772 (1996).

[8] Y. Yamada, T. Orii, I. Umezu, S. Takeyama, and T. Yoshida, *Jpn. J. Appl. Phys.* **35**, 1361 (1996).

[9] T. Yoshida, Y. Yamada, and T. Orii, p. 417 in *Technical Digest of the Inter. Electron Devices Mtg.*, San Francisco, CA, Dec. 8-11, 1996, IEEE.

[10] T. Makimura, Y. Kunii, and K. Murakami, *Jpn. J. Appl. Phys.* **35**, 4780 (1996).

[11] T. Makimura, T. Sakuramoto, and K. Murakami, *Jpn. J. Appl. Phys.* **35**, L735 (1996).

[12] T. Makimura, Y. Kunii, N. Ono, and K. Murakami, *Jpn. J. Appl. Phys.* **35**, L1703 (1996).

[13] T. Yoshida, personal communication. In the deposition experiments the laser pulse energy was 60 mJ, measured before the quartz entrance window. Assuming a

transmission factor of 0.91 and the 1 x 3 mm^2 area of refs. 7 and 8, this corresponds to $E_d \sim 1.8\ J/cm^2$.

[14] A. Matsunawa, S. Katayama, A. Susuki, and T. Ariyasu, *Trans. of Jap. Welding Res. Institute* **15**, 233 (1986).

[15] 0.003-inch x 3-inch #3 edge 1095 steel ribbon, tempered, polished, and blued; Amstek Metal, Joliet, Illinois.

[16] D. H. Lowndes, Christopher M. Rouleau, T. Thundat, G. Duscher, E. A. Kenik, and S. J. Pennycook, unpublished results and manuscript in preparation.

[17] G. Duscher, D. H. Lowndes, C. M. Rouleau, and S. J. Pennycook, Fall 1997 Meeting of the Materials Research Society, to be published in Mater. Res. Soc. Symp. Proc..

[18] D. B. Geohegan, *Appl. Phys. Lett.* **60**, 2732 (1992).

[19] See the article by D. B. Geohegan, G. Duscher, et al. in these proceedings.

Table 1. Mean diameters (and rms deviations) for ZnTe nanocrystals formed in N_2 or H_2 gas and collected at various target-substrate separations, D_{ts}, as measured by HRSEM or AFM.

Method	Gas	Pressure (torr)	D_{ts} (cm)	Diam. (rms dev.) (nm)
HRSEM	N_2	1.5	4	31.4 (14.1)
			8	19.2 (7.9)
			12	15.8 (4.7)
		10	4	25.1 (7.4)
AFM	N_2	0.15	10	1.05
		1.5	8	9.4
	H_2	1	10	1.36
		10	5	4.82

Figure Captions

Fig. 1. Areal density of Si nanoparticles vs nanoparticle diameter at D_{ts} = 10, 20, and 40 mm, for deposition using 500 ArF laser pulses at 1.04 J/cm^2 and a He pressure of 10 torr. Similar dependences of nanoparticle size on D_{ts} were obtained for P[He] = 1.5 and 4 torr.

Fig. 2 Average Si nanoparticle diameter (height) vs He gas pressure during ablation, at target-substrate separations D_{ts} = 10, 20, and 40 mm. For each D_{ts}, size distributions were measured at two locations on each substrate, believed to correspond to the center and left-of-center of the ablation plume (open symbols and dashed lines). The average is shown by the solid symbols and line. Results from refs. 7 and 10 also are shown.

Fig. 3 (Top) Atomic-resolution Z-contrast HRTEM image of a large ZnTe nanocrystal (center) with a small nanocrystal attached (lower right). Crystalline lattice planes are clearly seen in the interiors of both nanoparticles. (Bottom) Composition profile derived from spatially resolved EELS taken point-by-point across the larger ZnTe nanocrystal shown above (see text).

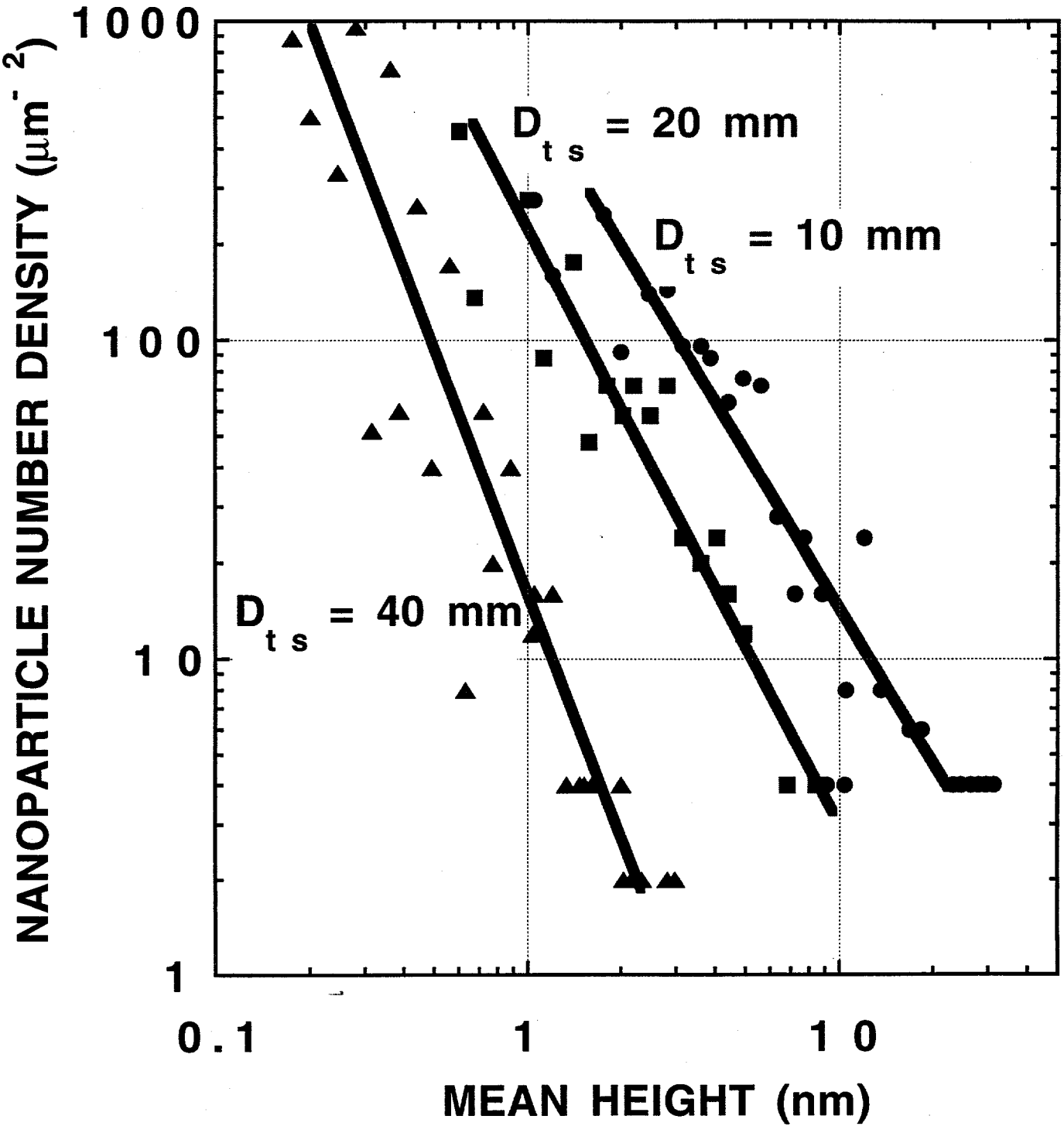
1000
100
10
1
NANOPARTICLE NUMBER DENSITY (μm⁻²)
D ts = 20 mm
D ts = 10 mm
D ts = 40 mm
0.1
1
10
MEAN HEIGHT (nm)

Figure 1

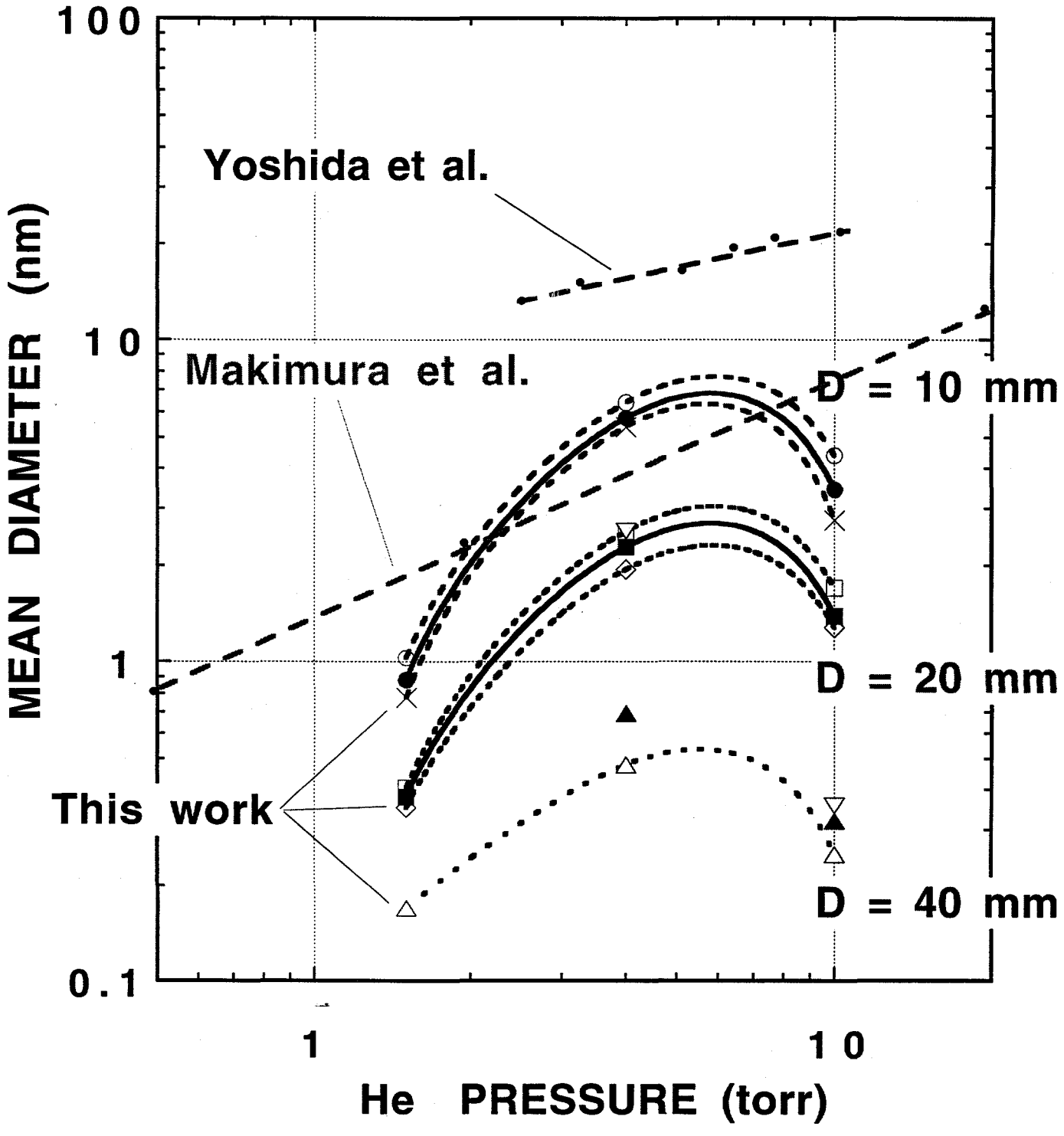
100
10
1
0.1
MEAN DIAMETER (nm)
Yoshida et al.
Makimura et al.
D = 10 mm
D = 20 mm
D = 40 mm
This work
1
10
He PRESSURE (torr)

Figure 2

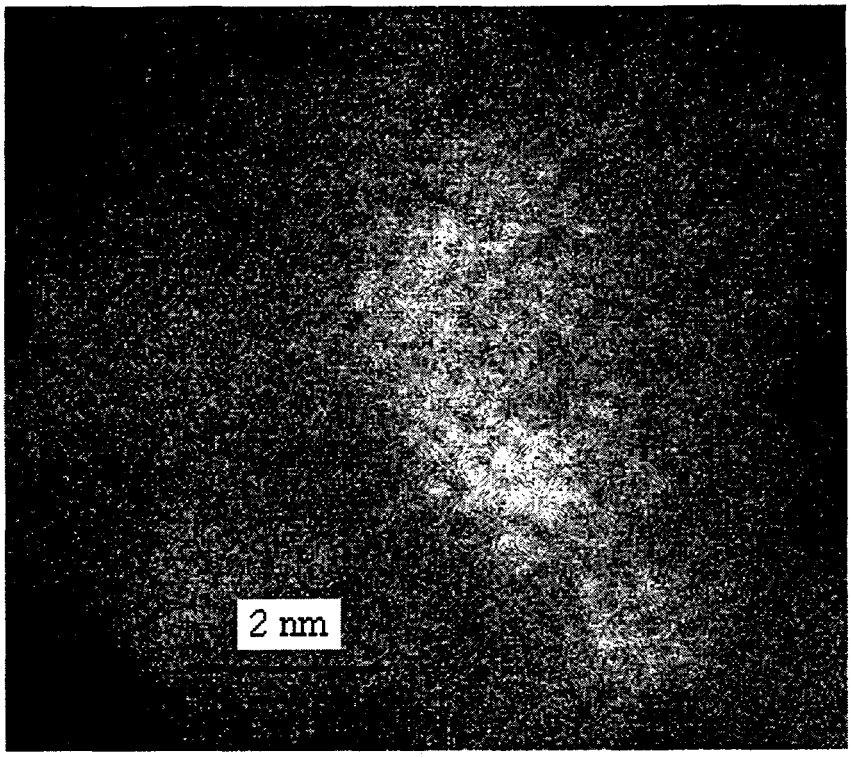
2 nm

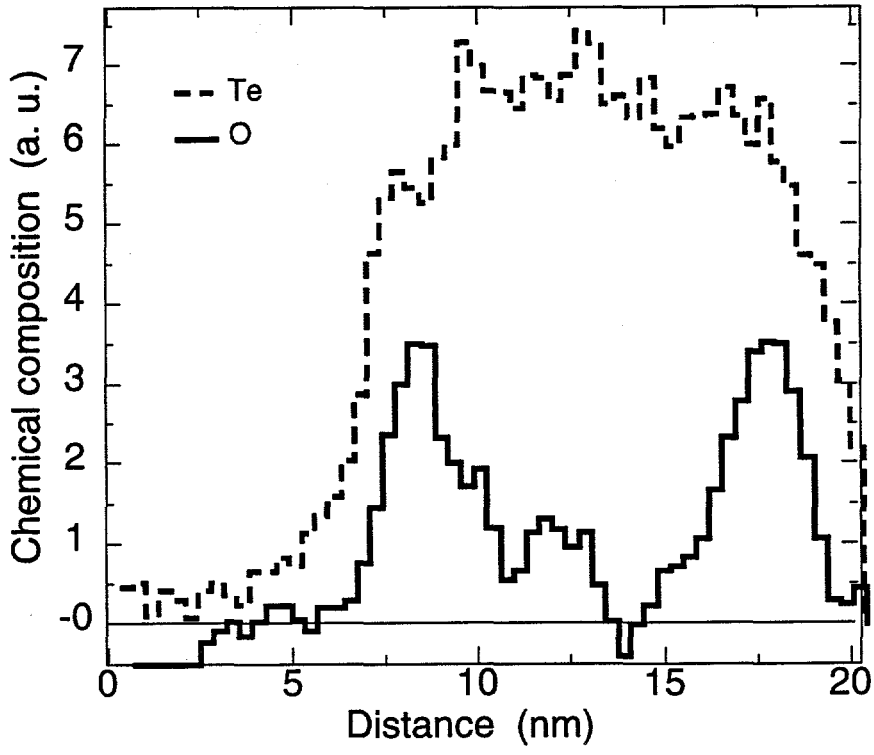
Te
O
Chemical composition (a. u.)
7
6
5
4
3
2
1
-0
0
5
10
15
20
Distance (nm)

Figure 3